Identifying fracture-controlled resonance modes for structural health monitoring: insights from Hunter Canyon Arch (Utah, USA)

Guglielmo Grechi[1,2], Jeffrey R. Moore[1], Molly E. McCreary[1], Erin K. Jensen[1], Salvatore Martino[2]

[1]Department of Geology and Geophysics, University of Utah, Salt Lake City, 84112, USA (UT)
5   [2]Department of Earth Sciences, Sapienza University of Rome, Rome, 00185, Italy

Correspondence to: Guglielmo Grechi (guglielmo.grechi@uniroma1.it)

Abstract. Progressive fracturing contributes to structural degradation of natural rock arches and other freestanding rock landforms. However, methods to detect structural changes arising from fracturing are limited, particularly at sites with difficult access and high cultural value where non-invasive approaches are essential. This study aims to determine how fractures affect
10   the dynamic properties of rock arches, focusing on resonance modes as indicators of structural health conditions. We hypothesize that damage resulting from fracture propagation may influence specific resonance modes that can be identified through ambient vibration modal analysis. We characterized the dynamic properties (i.e., resonance frequencies, damping ratios, and mode shapes) of Hunter Canyon Arch, Utah (USA), using spectral and cross-correlation analyses of data generated from an array of nodal geophones. Results revealed properties of nine resonance modes with frequencies between 1 and 12
15   Hz. Experimental data were then compared to numerical models with homogeneous and heterogeneous compositions, the latter implementing weak mechanical zones in areas of mapped fractures. All numerical solutions replicated the first two resonance modes of the arch, indicating these modes are insensitive to structural complexity derived from fractures. Meanwhile, heterogenous models with discrete fracture zones succeeded in matching the frequency and shape of one additional higher mode, indicating this mode is sensitive to the presence of fractures and thus most likely to respond to structural change from
20   fracture propagation. An evolutionary crack damage model was then applied to simulate fracture propagation, confirming that only this higher mode is sensitive to structural damage resulting from fracture growth. While examination of fundamental modes is common practice in structural health monitoring studies, our results suggest that analysis of higher-order resonance modes can be more informative for characterizing fracture-driven structural damage.

1 Introduction

25   Natural rock arches are rare and remarkable, culturally valued geologic landforms owing to their rarity, fragility, and beauty, as well as their significance to indigenous populations. Arches form and evolve over time in response to environmental and anthropogenic stresses whose weathering action can be aided by predisposing geological factors such as weak rock layers or rock mass fractures (Moore et al., 2020; Ostanin et al., 2017). Rock fractures nucleate and propagate in directions often reflecting principal stress orientations or following pre-existing discontinuities (Blair Jr, 1987; Bruthans et al., 2014;

1

30   Cruikshank and Aydin, 1994; Řihošek et al., 2018). As fractures grow to critical lengths, material is shed through partial failures at the arch lintel and abutments, sometimes resulting in self-sculpture of ideal arch forms (i.e., the inverted catenary) but often contributing to reduced stability and ultimate collapse (Moore et al., 2020). Understanding how rock mass fractures impact the stability of rock arches and other natural landforms is crucial for developing effective monitoring strategies aimed at their preservation.

35   Ambient vibration modal analysis of geologic landforms can provide crucial data supporting site characterization, stability assessment, and vibration risk analysis (e.g., Bessette-Kirton et al., 2022; Finnegan et al., 2022; Kleinbrod et al., 2019; Mercerat et al., 2021). Dynamic structural properties, such as modal frequencies, damping ratios, and deformation patterns at resonance (i.e., mode shapes) are controlled by material properties and boundary conditions (Chopra, 2013; Doebling et al., 1996), meaning accurate in-situ measurements provide data that can be used to create, calibrate or refine structural models

40   (Bottelin et al., 2017; Moore et al., 2018; Iannucci et al., 2020; Bessette-Kirton et al., 2022; Müller and Burjánek, 2023; Jensen and Moore, 2023). These dynamic properties can also be tracked over time for structural health monitoring (SHM) in order to detect and describe damage that may arise from natural and anthropogenic influences (Bottelin et al., 2013a, b; Burjánek et al., 2018; Colombero et al., 2021b; Geimer et al., 2022).

The small footprint and non-invasive nature of data generated using in-situ ambient vibration approaches makes such methods

45   particularly well-suited for applications at culturally valued, fragile geological features (e.g., rock arches and towers) as well as protected heritage sites (e.g., historic structures), where non-destructive techniques are required (Ceravolo et al., 2016; Conati Barbaro et al., 2024; Dzubay et al., 2022; Finnegan et al., 2021; Häusler et al., 2021a; Pau and Vestroni, 2013). The dynamic properties of an arch evolve with fracture propagation: as fractures grow the bulk material become softer (decreasing Young's modulus) and the landform may be increasingly separated from adjoining stable ground (increasing modal mass),

50   both resulting in resonance frequency decrease (Chopra, 2013; Clinton et al., 2006; Colombero et al., 2021b) Colombero et al., 2021b). In contrast, resonance frequencies may increase as material is shed during partial failure (decreasing modal mass). Such changes are anticipated to be detectable from ambient vibration modal analysis surveys, forming the basis for SHM techniques (Bottelin and Baillet, 2024; Çelebi, 2019; Doebling et al., 1996; Lévy et al., 2010). However, the nature of changes to mode shapes can be more challenging to predict and are likely to reflect complex, localized variations in structural properties

55   created by fractures of varying length, aperture, and stiffness.

Previous studies have successfully used experimental ambient vibration modal analysis to calibrate numerical models, providing input on structural parameters such as material properties and boundary conditions (Bessette-Kirton et al., 2022; Grechi et al., 2024). However, past applications have mainly modelled rock masses as homogeneous, isotropic continuous media. This assumption can be appropriate at sandstone arch and tower sites with few fractures and uniform lithology

60   (Finnegan et al., 2022; Geimer et al., 2020), but breaks down in cases of multiple lithologies or fractured rock masses, limiting application of the approach. Moreover, in the hypothetical case of progressive landform failure, the influence of discrete internal and bounding fractures grows increasingly significant as rock mass fracturing progresses, meaning a transition from an isotropic continuum to a discontinuous rock mass may be anticipated as failure approaches (Taruselli et al., 2021). These

cases of advanced failure with structurally relevant fractures are likely to be among the most critical for hazard analysis and mitigation (Zhang et al., 2020).

Here we present operational modal analysis and numerical eigenfrequency modelling for Hunter Canyon Arch, a unique natural arch located in southeastern Utah, that is deeply fractured at the interface of the lintel and cliff-side abutment. We hypothesized that these fractures influence the properties of certain resonance modes, and evaluated results from operational and numerical modal analyses to test this hypothesis. Comparison between an isotropic continuous model and field data fails for higher-order modes (i.e. above mode two), indicating that simple models do not replicate the observed fracture-controlled mechanical complexity of the arch. In contrast, numerical models implementing discrete weak mechanical regions in areas of mapped fractures matched key aspects of higher modes. Interestingly, all models were able to match the first two resonance modes, indicating that these are insensitive to structural complexity associated with fractures. Our results instead highlight how higher-order modes may be most sensitive to evolving fracture-controlled structural damage, and that once identified, these modes should be monitored over time to characterize structural changes caused by fracture propagation.

2. Study site and structural characterization

Hunter Canyon Arch (Lat/Long: 38.5063, -109.5928) is a large natural rock arch located 10 km southwest of Moab, Utah, composed of massive sandstone of the Jurassic Wingate Formation (Fig. 1a). The arch measures 35 m high, 4 m wide and spans 20 m at an azimuth of 30°N from the edge of a plateau. It is easily observed from the trail below, but access to the top requires a demanding overland hike. The lintel is deeply fractured where it abuts the adjoining cliff, with multiple intersecting discontinuities in this region (Fig. 1b, c) indicating potentially unstable conditions. The sharp and segmented geometry of the arch is inherited from the local geostructural setting and reflects comparably recent rockfall and partial collapse events sculpting the present-day form.

We performed a drone-based photogrammetry survey to construct a high-resolution point cloud of the study area from georeferenced images using the structure-from-motion software Agisoft Metashape (www.agisoft.com). The resulting point cloud was processed and cleaned using CloudCompare (www.cloudcompare.org) by applying a statistical outlier removal filter for general noise reduction. The output was then analyzed using the Matlab toolbox Discontinuity Set Extractor 3.0 (Riquelme et al., 2014), which allows for semi-automatic identification and classification of rock mass fractures through local statistical and cluster analyses. Five joint sets were recognized from this analysis (Fig. 1), including sub-horizontal bedding (S0) and four steeply dipping sets (dip direction/dip, respectively): S1 (187°N/82°), S2 (45°N/80°), S3 (124°N/83°) and S4 (082°N/85°). The geometry of the sub-vertical fractures creates a double-cusp shape in the area between the plateau and the arch (Fig. 1b), while two sub-vertical fractures and horizontal bedding partially isolate a rock volume on the cliff side of the abutment (S1 and S2, Fig. 1c). This fracture-bounded compartment is tilted toward the arch on the eastern side where its base is partially overhanging, and the aperture of the back fracture (S2) is highest. Similarly, the fracture adjoining the lintel and abutment (S1) is characterized by greatest aperture on the eastern side (Fig. 1c).
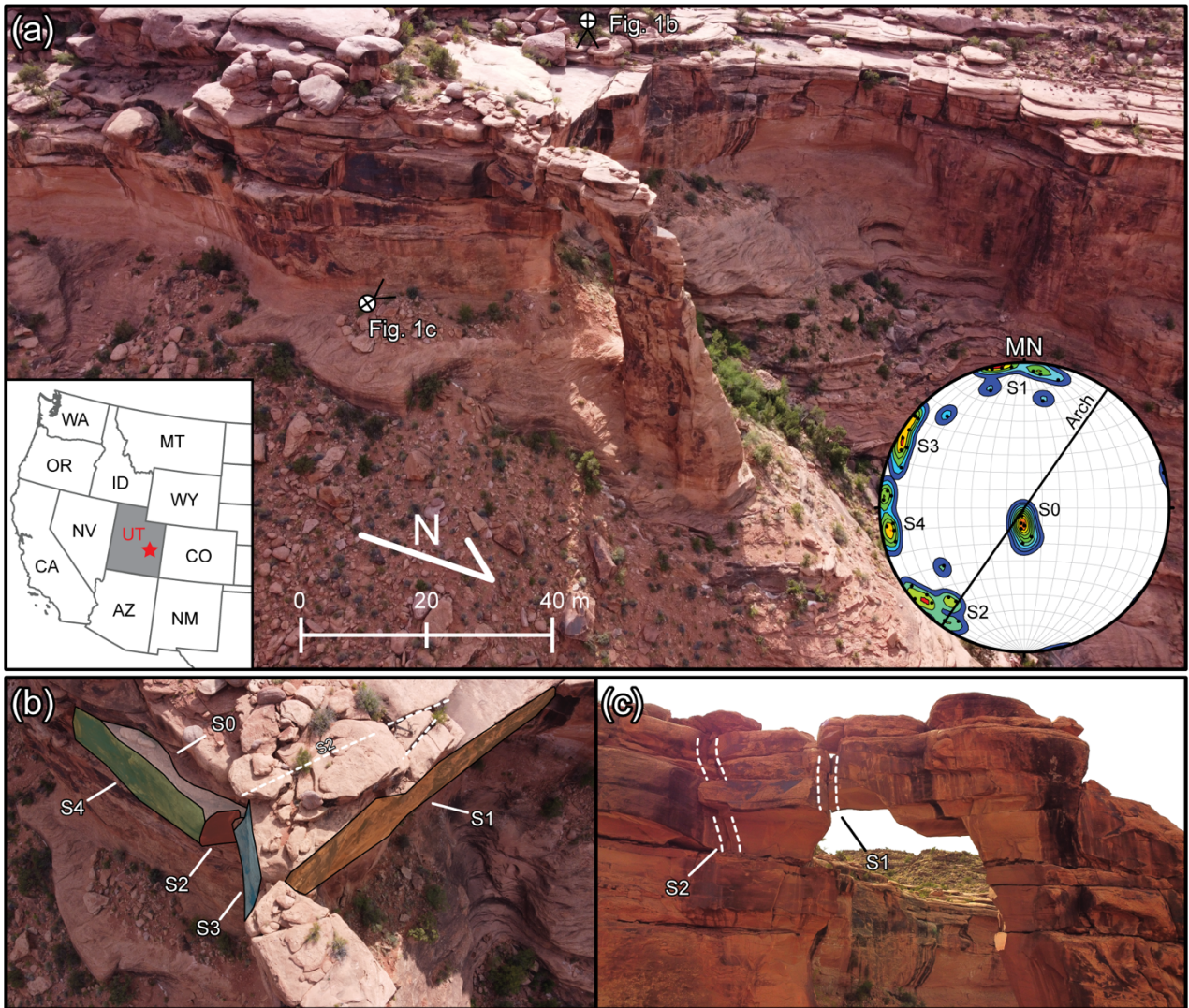
Figure 1: (a) Aerial overview of Hunter Canyon Arch located near Moab, Utah (location inset). Pole density contour plot in equal angle projection showing the five fracture sets identified from our remote survey is shown at lower-right inset. **(b, c)** Aerial views of Hunter Canyon Arch showing the main fracture traces (S0–S4) highlighted in different colors; camera locations for panels b and c are shown in a. Dashed lines show fracture traces of S1 and S2 without exposed surfaces.

3. Modal analysis methods

3.1 Nodal array field experiment

We deployed nine FairField Zland 5 Hz nodal geophones on October 9, 2022, recording three-component ambient vibration data during a 2-hour survey period (Fig. 2a, b). We placed eight stations in an approximately linear array with 3 m spacing to

cover the arch lintel and most prominent part of the fractured abutment (stations H01–H07). An additional station (H08) was deployed on the arch abutment, but due to the lack of suitable flat and debris-free bedrock, the geophone was positioned west of H07 interrupting the continuity of the linear array but still encompassing the fracture-bounded rock mass compartment closer to the arch. Station H09 was meanwhile positioned farther from the arch and abutment on the stable plateau to act as a
110 local reference (Fig. 2a). All sensors were levelled, aligned to magnetic north (10° N magnetic declination), and adhered to bare bedrock surfaces using mounting putty to ensure good ground coupling. Continuous ambient vibrations were recorded at a sampling frequency of 250 Hz between 18:00 UTC (10:00 MST) and 20:00 UTC (12:00 MST). Winds were calm during the experiment, minimizing environmental disturbance and thus improving signal-to-noise ratio of the vibration data. Other environmental factors, such as air temperature and relative humidity, varied little during the short duration of the experiment.

115 **3.2 Spectral and array cross-correlation analyses**

Ambient vibration data were analyzed for spectral content to identify resonance modes of Hunter Canyon Arch. The dataset was first examined to extract the longest undisturbed (e.g., due to wind, earthquakes, or anthropogenic noise) continuous time block for processing. This led us to reject the last 10 minutes of the recording. To process each array station and channel, we first removed the mean, linear trend, and applied instrument response correction via spectral division, finally bandpassing data
120 between 0.1 and 50 Hz. Horizontal channels were rotated to longitudinal (i.e., radial) and transverse (i.e., arch perpendicular) directions to align with the arch orientation (azimuth 30° N). Power Spectral Density (PSD) estimates of velocity were then computed following the approach of McNamara and Buland (2004). We used Welch's method (Welch, 1967) with stacked fast Fourier transforms of 60 s Hanning-tapered windows with 75 % overlap to reduce variance and smoothed over 0.1 Hz windows. We analyzed the resulting power spectra to manually identify spectral peaks that were hypothesized to represent
125 resonance modes of the arch (Fig. 2c).

To further characterize the identified spectral peaks, we performed frequency-dependent polarization analysis (Koper and Hawley, 2010). Polarization attributes (i.e., azimuth, incidence angle, and degree of polarization) of each spectral peak were identified and extracted, focusing on the degree of polarization (β^2) characterizing the extent to which particle motion is organized at the resonance frequencies. We additionally estimated the damping ratio (ζ) of identified resonance modes using
130 the random decrement technique (RDT) (Ibrahim, 1977), which fits an exponentially decaying sinusoid to the band-passed waveform approximating the free response of the system at each resonance frequency (Geimer et al., 2022). To characterize modal deformation patterns (i.e., mode shapes) associated with the identified resonance frequencies, we performed cross-correlation analysis using eight of the deployed array stations, omitting the reference station (H09). Mode shapes are essential parameters in SHM studies as they represent specific deformation patterns at each resonance frequency, hence describing the
135 relative displacement and phase relationships across different regions of the structure (Brincker and Ventura, 2015).
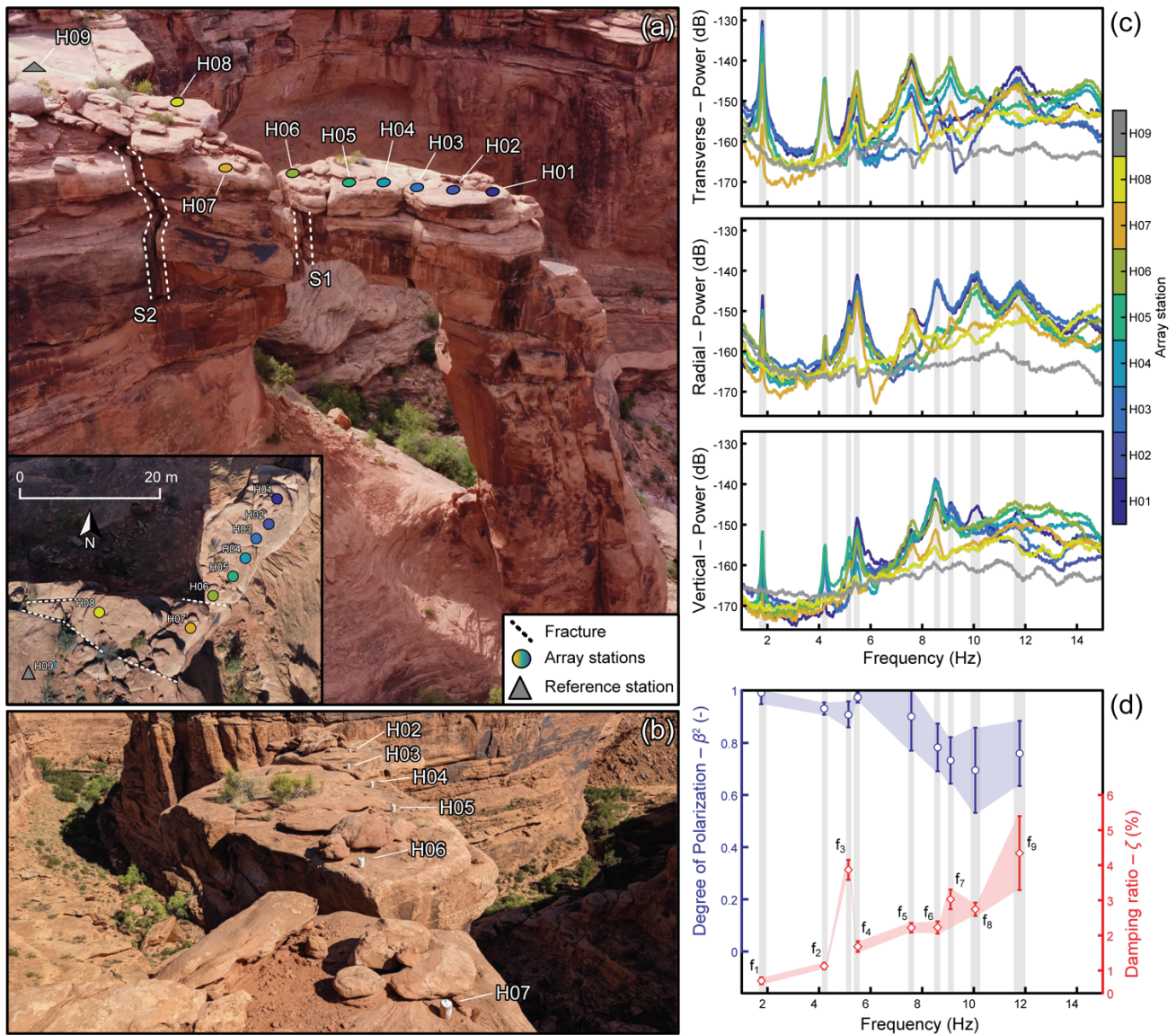
Figure 2: (a) Aerial view of Hunter Canyon Arch showing array stations (colored circles) and reference (gray triangle) as well as the fracture traces at the arch lintel and abutment (red dotted lines). Lower-left inset shows an orthophoto of the array and fracture traces. (b) Nodal geophones deployed on the arch (H01 is not visible) and the near fractured abutment. (c) Velocity Power Spectral Densities for all components (i.e., transverse, radial and vertical) and array stations. Decibel powers are relative to 1 m^2 s^{-2} Hz^{-1}. (d) Median and median absolute deviation values of the degree of polarization – β^2 (circles) and modal damping ratio – ζ (squares) for each of the nine identified resonance modes of Hunter Canyon Arch.

Cross-correlation modal analysis, also referred to as Natural Excitation Technique (NExT) (Farrar and James III, 1997), is a time-domain, output-only method used to estimate modal properties of vibrating structures by analyzing the cross-correlation functions between output response measurements under ambient excitation. We selected this analytical method over Frequency Domain Decomposition (FDD) and Stochastic Subspace Identification (SSI) techniques (Brincker et al., 2001; Van Overschee

and De Moor, 1996) on the basis of computational efficiency. The robustness of cross-correlation modal analysis, as compared to FDD and SSI has been previously demonstrated in comparative studies (Bessette-Kirton et al., 2022; Häusler et al., 2021a),

150   establishing it as a reliable approach for accurate modal property estimation of natural structures under ambient excitation. Array data were downsampled to 100 Hz, segmented into 5-minute tapered windows, and spectral whitening was applied prior to the cross-correlation of each station-pair (Bessette-Kirton et al., 2022; Lin et al., 2013). Maximum window amplitudes were used for time-domain normalization (Bensen et al., 2007) before stacking each station-pair to obtain cross-correlograms for the transverse-transverse (TT), radial-radial (RR), and vertical-vertical (ZZ) components. All cross-correlograms were then

155   filtered to 0.1 Hz bandwidth windows between 0.5 and 15 Hz, extracting the zero-time lag amplitude for each station-pair while omitting autocorrelation values. The resulting curve for each station enables visualization of mode shapes along the linear array, describing the amplitude and phase of relative modal displacements at each recording station (Fig. 3a). The curves were then normalized by the maximum Root Mean Square (RMS) amplitude and averaged to obtain a mean mode shape curve with standard deviation. Finally, for each resonance frequency identified from spectral analysis, we finally extracted the

160   average relative modal displacement for all components (i.e., TT, RR and ZZ) at all stations to plot 3D modal vectors on the Hunter Canyon Arch surface model (Fig. 3b) (Grechi et al., 2024).
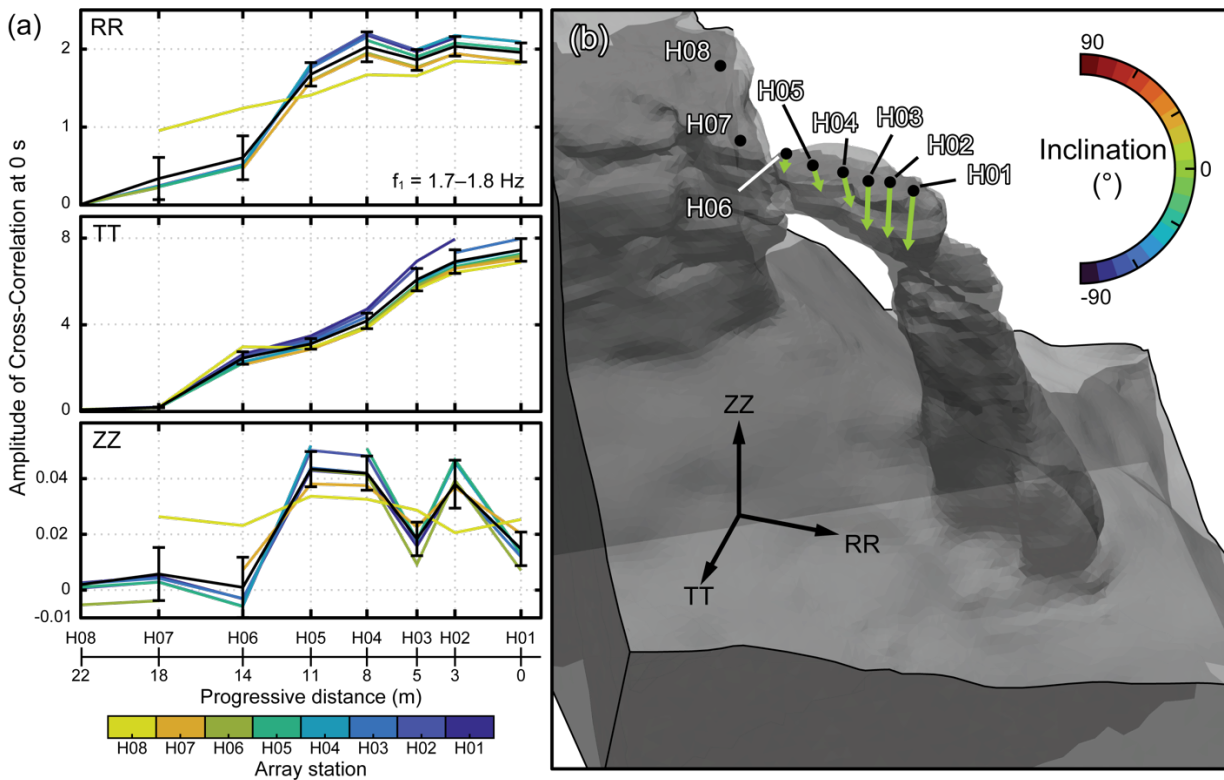
Figure 3: (a) Array cross-correlation results for the radial (RR), transverse (TT), and vertical (ZZ) components for the first
165   resonance mode of Hunter Canyon Arch (f1). Colored lines are RMS-normalized amplitude at each station relative to other array

stations. Black bold lines are the mean and standard deviation of the zero-lag cross-correlation amplitudes at every station. (b) 3D mode shape representation for f_1. To improve the overall visualization of mode shapes, vectors are color-coded according to their inclination angle, where 0° indicates horizontal inclination.

3.3 Numerical modal analysis

170   We performed 3D finite element eigenfrequency modal analysis (i.e., in the frequency domain and with no input excitation) to support structural characterization of Hunter Canyon Arch. The aim was to replicate the dynamic behavior of the arch by matching field data (i.e., resonance frequencies and mode shapes), thus constraining structural and material properties of the fractured rock lintel and adjoining cliff (Geimer et al., 2020). To accurately recreate the arch geometry, we used the high-resolution 3D surface model from our photogrammetric survey. General model improvements were performed in Meshmixer

175   (www.meshmixer.com) smoothing surface irregularities, filling holes from limited image coverage, and transforming the surface mesh into a solid 3D object that we imported in the finite element analysis software Comsol Multiphysics (www.comsol.com). Based on field surveying and results of spectral analysis, we cropped the final model to preserve the geophone array on the cliff-side abutment area where two major fractures exist (i.e., S1 and S2, Fig. 2a), removing distal areas not participating in modal deformation (e.g., reference station location H09) (Finnegan et al., 2022). Due to the lack of a

180   detailed geological description of fracture geometry, persistence, and aperture, as well as the presence and locations of rock bridges at depth, we adopted different numerical representations to simulate the arch dynamics.

In a first modelling attempt, we simulated the arch and adjacent cliff as isotropic, continuous, and homogeneous. We assigned material properties representative of Wingate Sandstone derived from previous studies (Moore et al., 2018): density (ρ) and Poisson's ratio (ν) were set as 2200 kg m^{-3} and 0.25, respectively, while Young's modulus (E) was allowed to iteratively vary

185   to match the first two measured resonance frequencies. All model outer boundaries were fixed at zero displacement to simulate the natural constraints of the surrounding rock mass. While continuum- modelling approaches have been successful in several past studies (Geimer et al., 2020), the assumption breaks down when structural complexities such as macroscopic fractures are involved (Burjánek et al., 2019; Moore et al., 2018). Subsequently, based on field observations of Hunter Canyon Arch, we implemented a heterogeneous numerical model through simulation of the two fracture regions cutting the arch lintel and

190   abutment (i.e., S1 and S2 in Figs 1c and 2a). Starting from the continuous model, the two fracture regions were simulated as discrete domains of reduced isotropic elastic modulus (E$_r$) (Burjánek et al., 2019; Grechi et al., 2024). We relied on our preliminary geologic model of the site, specifically on direct and remote surveys of fracture aperture and persistence, to generate these compliant mechanical zones. While S1 was modelled as a 1 m wide zone cutting entirely through the lintel, S2 was generated as a 2 m wide zone intersecting the rock mass for 8 m from the eastern side of the cliff and propagating to 8 m

195   depth (Fig. 5a). Both reduced stiffness domains were implemented via model partitioning using block elements with the same orientation as the real fractures. For material properties, we assumed ρ and ν were invariant from the homogeneous case and followed the previously described iteration for calibrating E$_r$ of both fracture zones to best match field data. Model calibration was obtained for E$_r$ values of 0.7 and 0.1 GPa for S1 and S2, respectively. To further explore structural complexity of the site and test different solutions for modelling fractures, we implemented two additional numerical models discretizing fractured

8

200   regions with the same extent of the reduced stiffness domains. In the first, fractures were modelled as open zones, represented as open discontinuities with constant aperture and no material properties assigned. The best-fitting between numerical and field data was achieved for a constant fracture aperture value of 0.1 m. For the second case, we implemented two thin elastic layers with isotropic surface stiffness (K_A) of 5 x 10^8 N m^{-3} to match measured resonance modes (Bottelin et al., 2017; Kulatilake et al., 2016). For all models, we extracted relative modal displacements in the transverse, radial and vertical

205   directions for the first four modelled resonance modes at points representative of array stations. Modelled mode shapes were then compared with experimental array cross-correlation results by analyzing the distribution of normalized vector magnitudes and angles (θ) between experimental and numerical vectors in 3D space. We calculated the angular difference between 3D experimental and numerical modal vectors as (Eq. 1):

$$\theta = \cos^{-1}\left(\frac{|u^T v|}{\|u\|\|v\|}\right) \tag{1}$$

Where u and v are the vectors being compared, $\|u\|$ and $\|v\|$ their magnitudes, and $|u^T v|$ their dot product.

210 **4. Results**

    Spectral analysis revealed nine consistent peaks between 1.8 and 11.5 Hz across the nodal geophone array. The absence of these spectral peaks at the reference station indicates they can be interpreted as resonance modes of Hunter Canyon Arch (Fig. 2c). The first and most prominent peak occurs at 1.8 Hz (f_1), with spectral amplitudes highest on the transverse component of arch stations (H01–H06) progressively decreasing toward the abutment (H07). The decrease in spectral power suggests the

215   fundamental mode of the arch is out-of-plane bending. The second mode ($f_2 = 4.2$ Hz) shows similar features with spectral powers mostly concentrated on the transverse component of array stations and a marked decrease in spectral amplitude at station H07. Modal damping ratios were estimated at 0.6 and 1.1 % for the first two modes, respectively, in agreement with results at other sandstone arch and tower sites in Utah (Häusler et al., 2021; Moore et al., 2019). No evidence of these first two modes is found further on the cliff abutment at station H08, strengthening their interpretation as fundamental resonance modes

220   of the arch. Multiple higher-order peaks are visible across the arch lintel and abutment stations (H01–H07) (i.e., 5.1, 5.3, 7.5, 8.5, 9.1, 10.1, 11.5 Hz). Two higher-order spectral peaks are visible at station H08 (i.e., $f_4 = 5.3$ and $f_5 = 7.5$ Hz). Damping ratios were also estimated for these higher-order modes, indicating an increasing trend with mode order (Fig. 2c). Only mode three exhibits an unexpectedly high damping ratio of 3.8 %, which is 2 to 3 times greater than adjacent modes (i.e., modes two and four have damping ratios of 1.1 and 1.5 %, respectively). We computed the median β^2 and median absolute deviation

225   values at each resonance mode for all array stations. The analysis highlighted median β^2 values in the range 0.7–1, indicating highly polarized motion indicative of organized modal deflection (Fig. 2c).

    Results of cross-correlation analysis allowed us to describe mode shapes associated with resonance frequencies of the arch identified from spectral analysis (Fig. 4). The first two modes represent first- and second-order transverse bending and feature no involvement of the abutment station H08 (Fig. 4a and b). Higher-order modes are characterized by more complex modal

9

deflection patterns, except for mode six which represents a first-order bending mode in the vertical direction (Fig. 4f). Mode shape complexity arises starting at modes three and four, where modal vectors show greater variability between arch stations as well as involvement of the abutment and fracture zone, as can be observed by the higher amplitude of modal displacements at station H07 (Figs 4c and d). Starting from these two modes and higher, strong similarity between stations H06 and H07 (i.e., the two stations at the transition from arch to abutment) can be observed both in modal vector orientation and magnitude. At mode five, for example, a second-order horizontal bending mode with node point at the middle of the arch, stations H07 and H08 show in-phase modal vectors characterized by comparable magnitude and orientation with stations located on the arch (Fig. 4e). Mode shapes for the last three identified resonance modes are characterized by a complex distribution of modal vectors, mostly concentrated in the radial and vertical directions, but also involving the arch abutment.

To improve our understanding of fracture control on arch dynamics, we compared results from continuous and heterogenous numerical models with field data. The heterogeneous model of Hunter Canyon Arch implemented using two reduced stiffness domains is shown in Figure 5a. For both numerical solutions we obtained several higher-order and complex resonance modes that showed poor correspondence with cross-correlation results. For this reason, we selected to analyze only those modes characterized by the highest relative modal mass (RMM) values (Fig. 5b). This direction-dependent parameter is frequently employed in engineering studies as it measures the extent of mass participation at each resonance mode, allowing for assessment of the significance of specific eigenmodes in describing the dynamic behavior of a structure (Aenlle et al., 2021; Mayes et al., 2015). For the continuous case, we were able to achieve a good match to the first two measured resonance modes in both frequency and mode shapes implementing an isotropic Young's modulus of 2.3 GPa, which is comparable to past results at sandstone arches and towers within the Wingate Formation (Geimer et al., 2020; Moore et al., 2019). However, modelled higher-order modes failed to reproduce field measurements in terms of frequency and mode shapes. The only exception is represented by the similarity between modelled mode four and measured mode six (i.e., first-order vertical bending mode). In this case, although the modelled mode order is not the same as field data and no evidence of third and fourth measured modes was found, the continuous model predicts a first-order vertical bending mode at 6.8 Hz (i.e., 20 % lower than the measured frequency). Therefore, due to the observed similarities in modal properties, we compared modelled mode four with measured mode six to further assess consistency in the vertical bending response predicted by numerical models. The same three eigenmodes of Hunter Canyon Arch are well resolved by the heterogeneous model implemented with fracture zones S1 and S2 (Fig. 5c). The presence of reduced stiffness domains simulating the compliant fractures within the model does not strongly affect either the frequency or shape of the first two resonance modes of the arch. However, differences arise for the third modelled mode, where the inclusion of fractures yields a good match in frequency and mode shape to the third measured mode. The improved performance of the heterogeneous model in replicating the third resonance mode is also indicated by the distribution of normalized modal displacement vector amplitudes and angular differences between numerical and experimental vector orientations (Fig. 6). Among the analyzed modes, we found that mode three highlights the better match of all heterogenous models when implementing discrete weak layers in areas of mapped open fractures (i.e., reduced stiffness domains, open zones and thin elastic layers), with average angular differences in the range 8–30°. Conversely, the continuous

numerical model failed to resolve this resonance mode as pointed out by differences in modal vector orientations up to 60°
(Fig. 6).

To further investigate the contribution of fractures and the control they exert on the dynamic response of natural rock landforms, we created an evolutionary crack-propagation model for Hunter Canyon Arch (Fig. 7). Starting from a hypothetical continuous-isotropic stage (T0), for which no fractures were implemented, we simulated structural damage as a sequence of discrete stages with increasing crack depths (T1–T5) following a top-down propagation pattern to reach the actual site conditions (T6). This crack evolution pattern was implemented based on field observations. However, this assumption is likely also valid at sites characterized by similar geometrical, boundary and fracture conditions where, for example, bounding or abutment fractures often exhibit similar propagation characteristics because of local tensile stress concentrations (Moore et al., 2020). For each modelled damage stage, we derived resonance frequencies and mode shapes to evaluate potential changes in the dynamic behavior of the arch due to increased crack propagation. Results show that mode three is characterized by a greater sensitivity to fracture propagation than the other modes. In fact, while modes one, two and four undergo small shifts in their resonance frequency values (± 2 %) with increasing crack depth, mode three features a decreasing trend up to –12 % at stage T6 (Fig. 7b). Meanwhile, the progressive deepening of S1 and S2 creates a marked shift in relative modal displacements of mode three, with the shape at stage T6 closely matching our experimental results (Fig. 7c–f). On the other hand, other modelled resonance modes undergo smaller changes in deformation patterns, with numerical results that are comparable to field data for almost every damage stage, indicating their relative insensitivity to fracture depth.
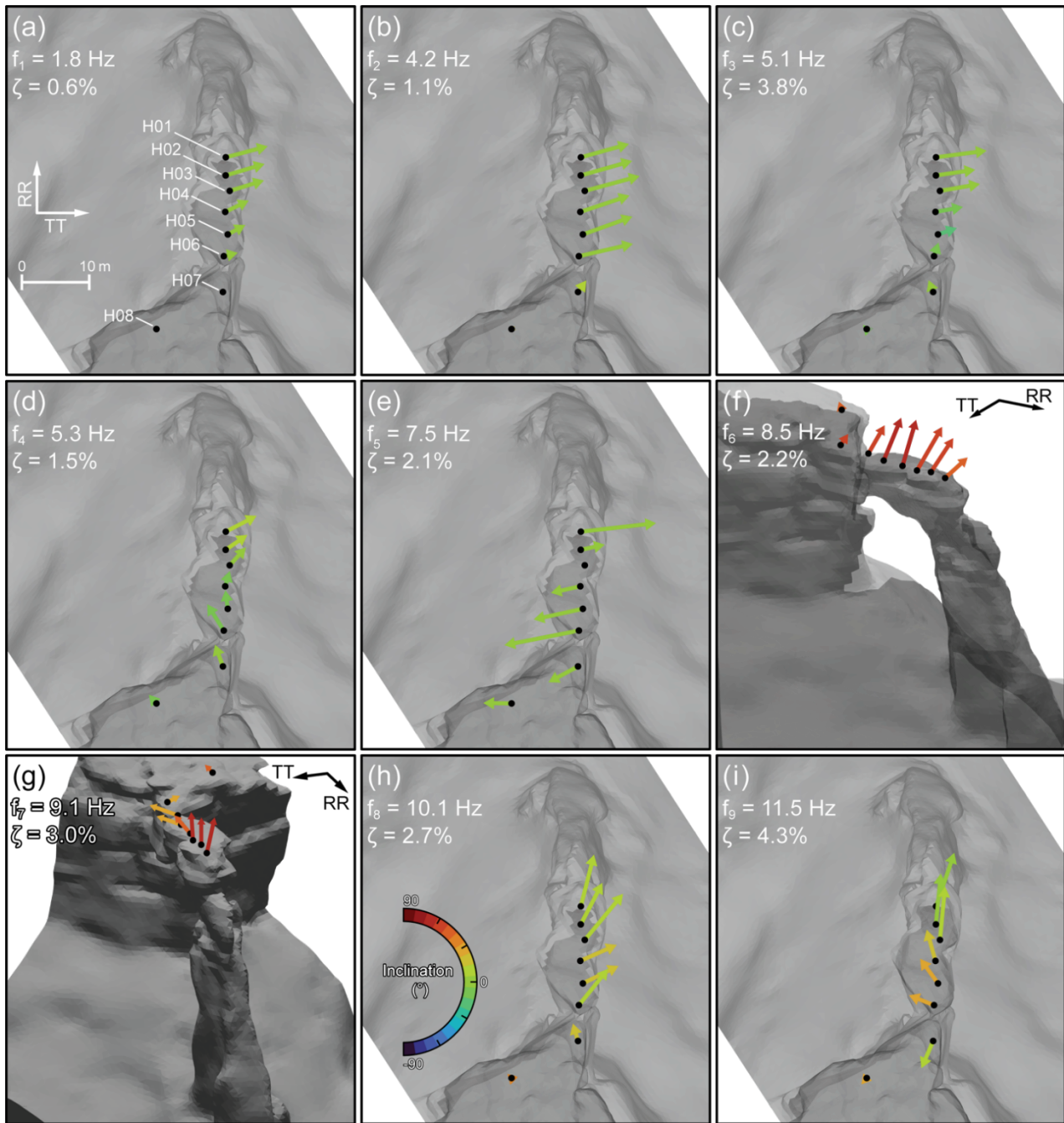
11

Figure 4: (a–i) 3D representation of the nine resonance modes of Hunter Canyon Arch via cross-correlation analysis. Arch models in panels f and g are rotated relative to other panels to improve visualization of prevalent vertical in-plane deformation patterns. Modal vectors are normalized to the maximum array amplitude. To improve the overall visualization of mode shapes in a 2D view, vectors are colored according to their inclination angle, where 0° indicates horizontal inclination.
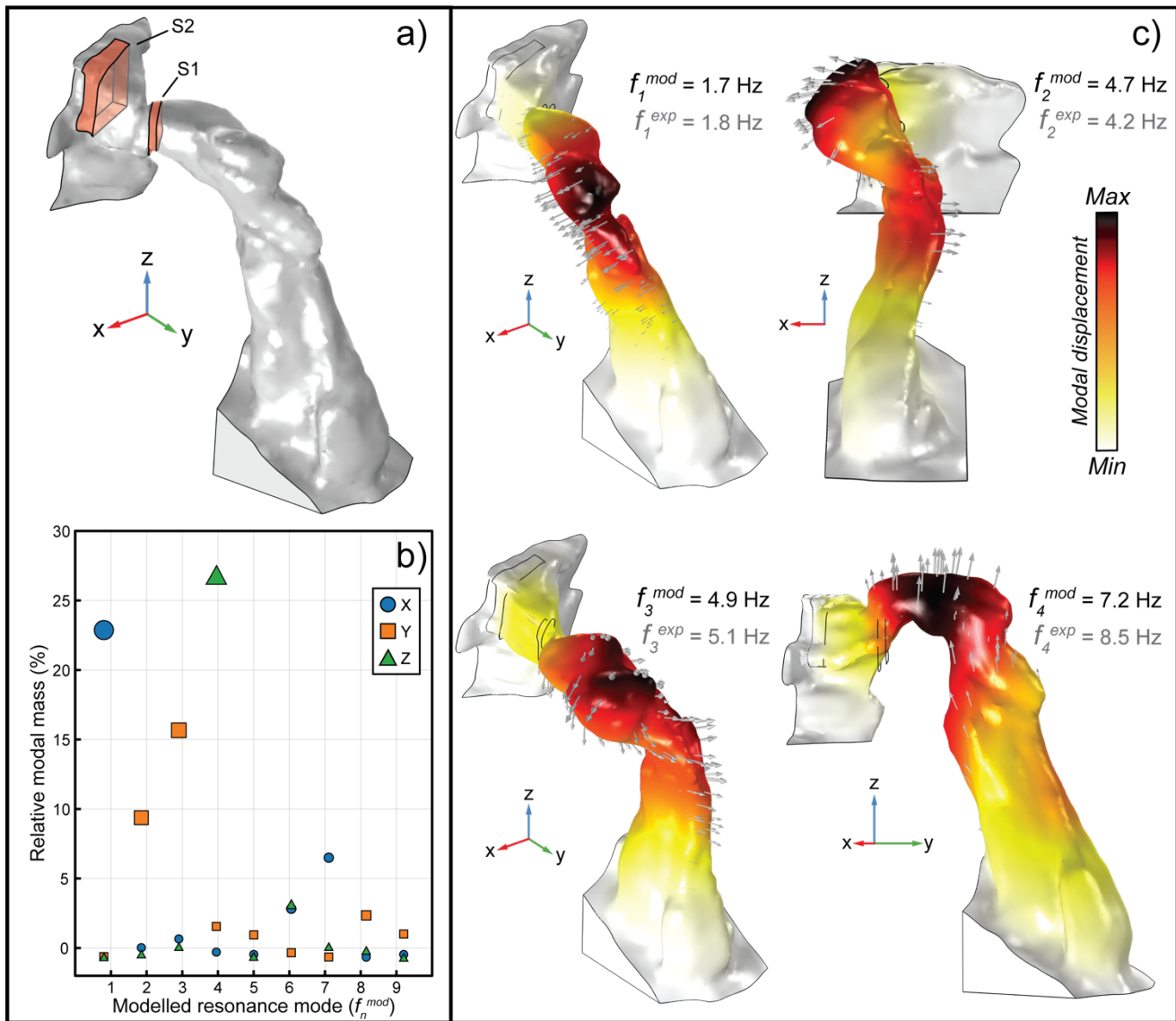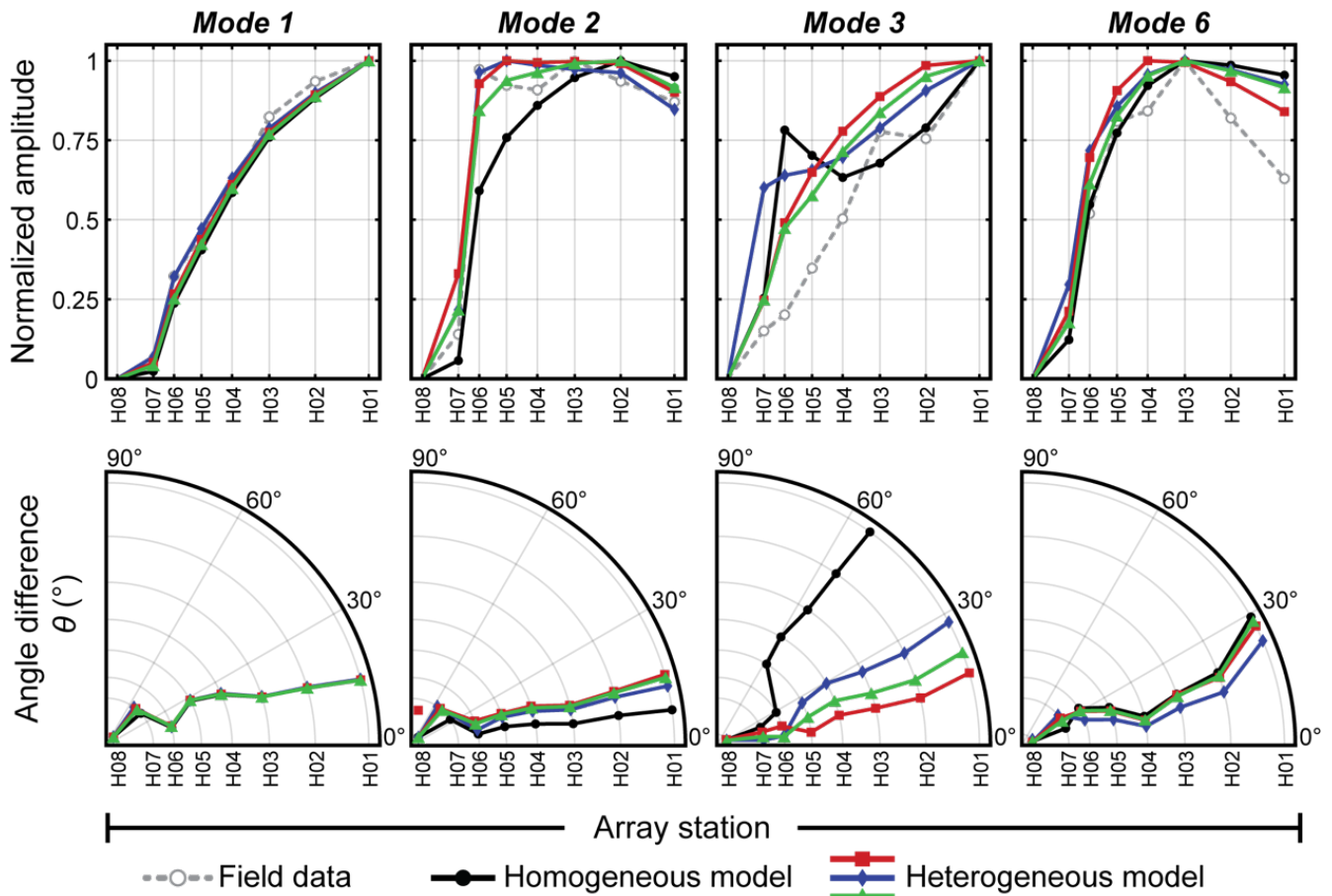
285

Figure 5: (a) 3D finite element model of Hunter Canyon Arch with detail of S1 and S2 implemented as discrete volumes of reduced elastic modulus (red zones). (b) Relative modal masses in X, Y and Z derived for all modelled resonance modes using the heterogeneous model. (c) Numerical modelling results (modes 1–4) for the reduced stiffness heterogeneous model. Modelled mode shapes and frequencies are shown for each mode (f_n^{mod}), while corresponding measured resonance frequencies are given in gray (f_n^{exp}). Model deformation, colormaps and arrows show zero-phase displacement normalized relative to each mode. Modelled mode 4 (f_4^{mod} = 7.2 Hz) is compared to measured mode 6 (f_6^{exp} = 8.5 Hz) as numerical analysis failed to replicate measured modes 4 and 5.

Figure 6: Comparison between field data (e.g., Fig. 4) and numerical modelling representations of Hunter Canyon Arch. For each resonance mode, normalized modal displacement amplitude (upper row) and angular difference (θ) between modelled and measured 3D modal vectors are shown for all array stations (lower row). Three different approaches were tested for simulating rock mass structural-mechanical heterogeneity: reduced stiffness domains (red squares), thin elastic layers (green triangles), and open fractures (blue diamonds).
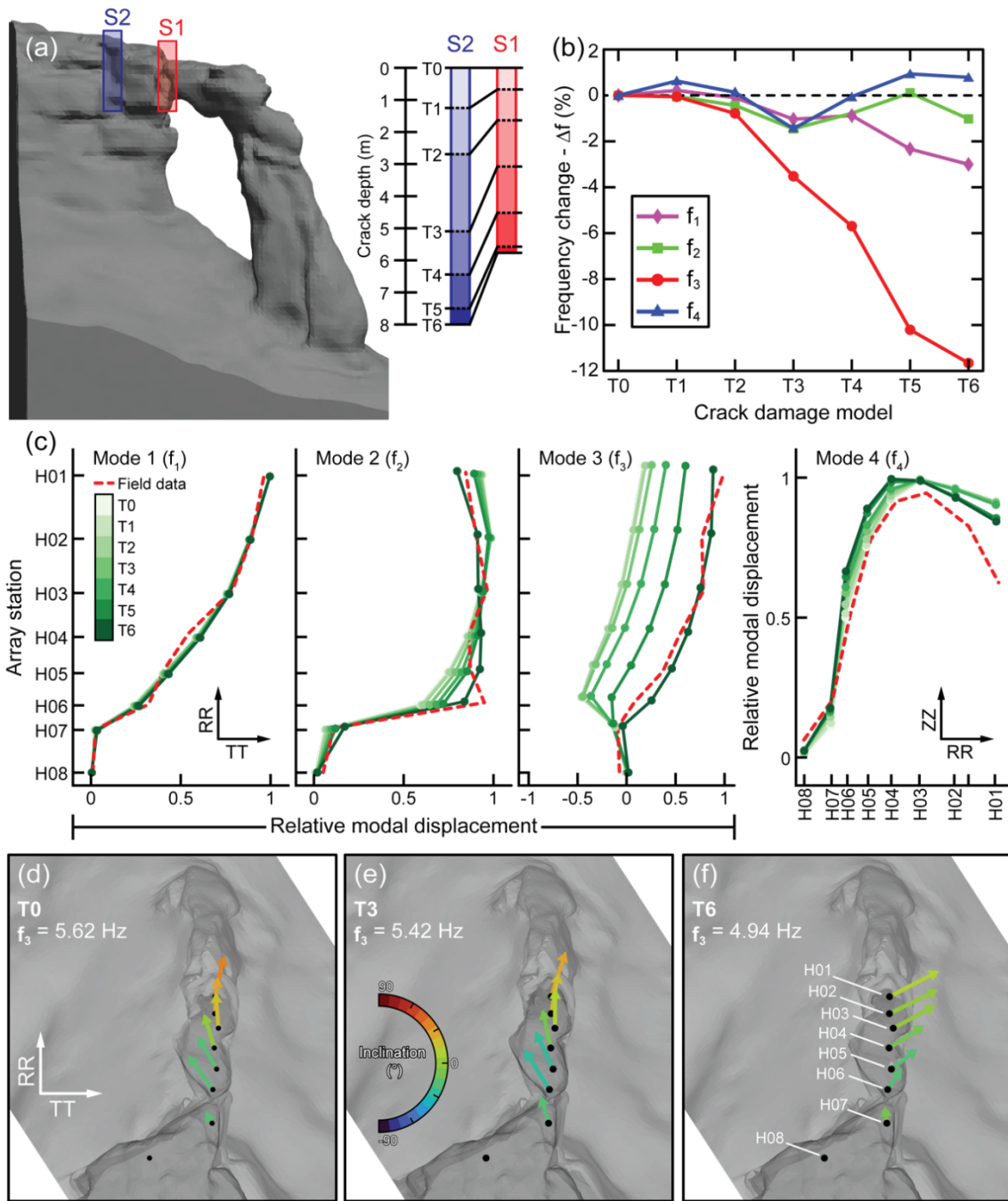
Figure 7: Evolutionary crack damage model describing the effect of increasing crack depth on resonance modes of Hunter Canyon Arch. (a) 3D model of the arch with location of the two modelled fractures (S1 and S2). Inset sketch describes the seven modelled crack depth stages (T0–T6): T0 features no fractures (homogeneous case) while T6 reflects actual site conditions. (b) Modelled resonance frequency change for f_1 to f_4 as a function of increasing crack depth. (c) Progressive change in 2D resonance mode shape for the four modelled modes at different crack propagation stages. Experimental mode shapes are also provided (red dashed lines) to compare field and numerical modelling results. (d–e) 3D modelled mode shapes for f_3^{mod} at stages T0, T3, and T6; mode shapes are not shown for f_1^{mod}, f_2^{mod} and f_4^{mod} as they do not vary with crack propagation.

15

5. Discussion

Ambient vibration array data generated at Hunter Canyon Arch enabled identification and characterization of nine resonance
modes of the natural sandstone arch. This is the largest number of modes measured until now at a natural arch site (Geimer et
al., 2020), demonstrating the value of array-based field data. We observed almost no involvement of the abutment stations
H07 and H08 in modal deflection patterns of the first two resonance modes of the arch. However, starting at mode three, we
find greater correspondence between stations H06 (i.e., the last station on the arch) and H07, with modal vectors having
comparable magnitudes and orientations. Hence, experimental data show how the modal deformation field related to higher-
order resonance modes propagates to the cliff side across fracture S1 (i.e., the discontinuity dissecting the abutment), indicating
these areas are elastically connected.

Similar evidence can be derived from analysis of damping ratios. The first two resonance modes show low damping ($\leq 1 \%$)
in good agreement with results obtained at other sandstone arch sites (Geimer et al., 2020; Häusler et al., 2021a; Moore et al.,
2019). These low damping values indicate that seismic energy is trapped within the structure and unable to propagate to the
surrounding rock mass due to the minimal contact area of the abutment and base surfaces compared to the overall modal mass
of the arch (Häusler et al., 2021b). Starting from mode three, higher-order resonance modes exhibit an increasing trend in
damping ratios (Fig. 2c). This result is not unexpected since complex deformation patterns, generally characterized by a greater
number of node points, can aid in energy dissipation through relative motion and material-dependent internal friction
mechanisms. However, mode three itself shows a marked increase in damping (up to 3.8 %), indicating some additional,
frequency-dependent seismic energy dissipation mechanism. We hypothesize this change could arise from increasing
participation of the abutment fracture area, and corresponding fracture shear and normal compliance, in modal deflection of
the arch. In structural engineering, it is well-documented that frictional interfaces, such as joints and connections, contribute
to energy dissipation due to micro-slip and frictional losses under dynamic loading (Cimellaro, 2023; Lazan, 1968). This
phenomenon, often referred to as interface or slip damping, is critical in dynamic analysis and structural design. In engineering
geology, the role of fractures in modifying energy dissipation mechanisms is less extensively studied, and there is a higher
degree of uncertainty due to the complex nature of rock fractures (i.e., geometry, properties, contact areas). Despite this, it is
reasonable that frictional interactions at fracture interfaces, as well as surface roughness, can contribute to increased energy
dissipation within rock masses (Bandis et al., 1983; Goodman, 1980; Habaraduwa Peellage et al., 2024).

The increase in energy dissipation at the fracture scale is also indirectly supported by our numerical modelling results. Although
all models (i.e., continuous and heterogeneous) were able to resolve the first two (as well as the sixth) resonance modes of the
arch, suggesting their mode shapes are independent of the contribution driven by discrete compliant zones, only the
heterogeneous models could match the frequency and shape of mode three. Changes in internal mechanical and boundary
conditions (i.e., the introduction of fractures) did not affect mode shapes or frequencies for the first two resonance modes,
demonstrating the insensitivity of these low-order modes to the modelled fractures. It is worth pointing out that numerical
representation of fractures is a complex approximation as it involves many inherent simplifications and assumptions, especially

16

in their geometrical discretization and mechanical characterization (Burjánek et al., 2019; Colombero et al., 2018). For this reason, after accurate reconstruction of the arch geometry, we adopted different numerical solutions for implementing fractures with the aim of testing the hypothesis of a fracture-controlled influence on the modal behavior of the arch. Our results suggest that, regardless of the adopted approach and parametrization (i.e., reduced stiffness domains, thin elastic layers, open fractures), the introduction of discrete compliant domains provides a better fit to experimental data than the continuous model for the third resonance mode of the arch. It is worth underlining that real fractures are characterized by more complex and heterogeneous structural-mechanical features than what was numerically recreated in this study, as they can include rock bridges, voids, and material infillings, while their aperture may vary strongly with depth (Colombero et al., 2017). Nonetheless, the results we obtained improved our engineering geological model of the site by providing evidence for the role of fractures in affecting the modal behavior of the arch.

Our evolutionary crack damage modelling indicated that the third resonance mode of the arch was particularly sensitive to simulated crack propagation at the arch abutment, undergoing substantial changes in frequency (– 12 %) and mode shape (Fig. 7). Other modes exhibited less change (frequency shifts around ± 2 %), and especially the first two modes were comparably insensitive to simulated crack propagation. These findings highlight the sensitivity of higher-order resonance modes to localized rock mass damage, and additionally suggest that fundamental resonance modes might not always be the most informative proxies for detecting and monitoring the evolution of structural damage in natural rock landforms. Based on the results obtained at this site, we hypothesize that when a finite number of discrete fractures actively constrain the mechanical and dynamic behavior of the landform, structural damage driven by progressive growth of these fractures could be undetectable by fundamental resonance mode monitoring. Instead, where well-developed dense fracture networks exist and the role played by individual fractures becomes less relevant, substantial changes in bulk properties may arise causing variation in the structure's full dynamic response across many modes (Grechi et al., 2024).

The combination of our experimental and numerical modelling results indicates that higher-order resonance modes may be more sensitive to localized structural damage. This outcome is particularly relevant in relation to monitoring and conservation of damaged structures, as in structural health monitoring applications the first resonance modes are often considered the most informative to detect and track damage (Azzara et al., 2020; Clinton et al., 2006; Colombero et al., 2018, 2021a; Häusler et al., 2021b). However, since well-developed discontinuities serve as preferential pathways guiding damage and rock mass failure evolution, the consideration of fracture-sensitive, higher-order resonance modes could be valuable for identifying and monitoring progressive degradation of natural rock landforms at early stages. In particular, the evolution of fractures due to progressive failure could be assessed by discerning irreversible changes in modal properties of fracture-sensitive resonance modes (Alaei et al., 2023). It is worth noting that although higher-order modes can provide valuable insights for the detection and monitoring of structural damage, their identification and characterization can pose challenges due to general lower energy levels and more complex shapes compared to fundamental modes (Häusler et al., 2021a).

Our results also indicate the importance of array-based field data in providing a more robust analytical framework compared to single-station measurements for the investigation of sites characterized by complex structural and boundary conditions.

375 Single-station ambient vibration data have been successfully used in the past in combination with 3D finite element analysis to characterize the dynamic behavior of freestanding rock structures (Finnegan et al., 2022; Geimer et al., 2020; Moore et al., 2019; Starr et al., 2015). These in-situ measurements have proved suitable for identifying and monitoring modal parameters, which can be used to calibrate numerical models by matching experimental and modelled results to derive rock mass scale material properties and describe modal strain fields (Bessette-Kirton et al., 2022; Moore et al., 2018). However, this approach

380 can fail when dealing with complex settings where rock mass fractures can act as primary factors of structural heterogeneity (Grechi et al., 2024). Instead, the deployment of dense sensor arrays yields more comprehensive spatial coverage which is crucial for identifying and characterizing resonance modes and relative modal shapes, particularly in discriminating higher-order modes or changes in modal shapes due to structural heterogeneities. Therefore, array data are valuable at sites with a high degree of structural complexity to provide accurate description of modal behavior, including the influence of fractures,

385 where initial array measurements can highlight fracture-controlled modes and repeated surveys can reveal structural changes associated with damage evolution.

6. Conclusions

This study investigated how fractures influence the dynamic behavior of a natural rock arch, with the hypothesis that specific resonance modes would be more affected by fractures and fracture propagation due to localized compliance effects.Ambient

390 vibration array data from Hunter Canyon Arch, Utah, allowed us to characterize the properties of nine resonance modes, including modal frequencies, damping ratios and mode shapes. Results of operational modal analysis supported our hypothesis, showing that fractures at the arch abutment affect the third resonance mode of the arch as evidenced by significant changes in damping and mode shape. Numerical modelling further corroborated these findings, demonstrating that only models incorporating fractures could replicate the observed dynamic behavior of the arch and specifically mode three, and that this

395 mode was most sensitive to simulated fracture propagation exhibiting substantial changes in frequency and mode shape. Results of spectral and cross-correlation analyses showed no involvement of abutment or cliff sectors at the first two resonance modes. While the first two resonance modes exhibit low damping ratios, in agreement with results from other sandstone arch sites, we observed a strong increase in damping at mode three that we interpret as resulting from added energy dissipation mechanisms associated with fracture compliance. We tested various numerical modelling approximations of the site, including

400 a homogenous model (i.e., without fractures) and heterogeneous models featuring different fracture configurations, as well as an evolutionary crack propagation simulation. Results show that the first two modelled modes are insensitive to the simulated fractures. Heterogeneous models were able to better match field data for the third mode, but could not match all, indicating remaining limitations of our models in capturing the complexities of spatially varying fracture geometry and compliance.

Despite the complexities in representing real fractures numerically, our results underscore the primary role of fractures in

405 modifying the dynamic behavior of this natural arch at a specific resonance mode. In this sense, the significance of fracture-sensitive resonance modes in structural health monitoring is noteworthy because, while traditional approaches often prioritize

the first or fundamental resonance modes, our study suggests that investigating higher-order modes may be crucial for identifying and monitoring the evolution of structural damage of natural rock landforms, especially where macroscopic compliant fractures are involved. These findings additionally emphasize the importance of generating in-situ ambient vibration array data, particularly at sites with substantial structural complexity. The approach we present here, integrating array-based experimental modal analysis and numerical eigenfrequency modelling, not only enhanced our understanding of the dynamic behavior and structural conditions of the arch, but also provided useful insights that can contribute broadly to refined structural health monitoring practices. The integration of experimental measurements and numerical modelling is essential for comprehensive assessment of the dynamic behavior of natural rock landforms, particularly those featuring complex fracture networks, paving the way for improved conservation strategies and risk management at natural heritage sites. Furthermore, calibrated numerical models (i.e., constrained by high resolution structural characterization and site-specific geophysical investigations) are, in turn, crucial for scenario analyses where the role of preparatory processes and triggering actions can be weighed and used to guide preservation solutions.

Code and data availability

The 3D photogrammetric model generated in this study is available for download at: https://skfb.ly/oILIM. Seismic data are available at: https://doi.org/10.7914/SN/5P_2013.

Author contribution

Conceptualization: GG, JRM, SM — Data curation: GG, JRM, EKJ — Formal analysis: GG — Funding acquisition: JRM — Investigation: GG, JRM, MEM — Methodology: GG, JRM — Project administration: GG, JRM — Software: GG, JRM, EKJ — Supervision: JRM — Validation: GG, JRM — Visualization: GG, JRM — Writing – original draft: GG, JRM — Writing – review & editing: GG, JRM, MEM, EKJ, SM.

Competing interests

The authors declare that they have no conflict of interest.

Acknowledgements

References

435   Aenlle, M., Juul, M., and Brincker, R.: Corrigendum to "Modal Mass and Length of Mode Shapes in Structural Dynamics," Shock and Vibration, 2021, 9821852, https://doi.org/10.1155/2021/9821852, 2021.

Alaei, A., Hejazi, M., Vintzileou, E., Miltiadou-Fezans, A., and Skłodowski, M.: Effect of damage and repair on the dynamic properties of Persian brick masonry arches, The European Physical Journal Plus, 138, 231, https://doi.org/10.1140/epjp/s13360-023-03781-0, 2023.

440   Azzara, R. M., Girardi, M., Iafolla, V., Padovani, C., and Pellegrini, D.: Long-Term Dynamic Monitoring of Medieval Masonry Towers, Frontiers in Built Environment, 6, https://doi.org/10.3389/fbuil.2020.00009, 2020.

Bandis, S. C., Lumsden, A. C., and Barton, N. R.: Fundamentals of rock joint deformation, International Journal of Rock Mechanics and Mining Sciences & Geomechanics Abstracts, 20, 249–268, https://doi.org/10.1016/0148-9062(83)90595-8, 1983.

445   Bensen, G. D., Ritzwoller, M. H., Barmin, M. P., Levshin, A. L., Lin, F., Moschetti, M. P., Shapiro, N. M., and Yang, Y.: Processing seismic ambient noise data to obtain reliable broad-band surface wave dispersion measurements, Geophysical Journal International, 169, 1239–1260, https://doi.org/10.1111/j.1365-246X.2007.03374.x, 2007.

Bessette-Kirton, E. K., Moore, J. R., Geimer, P. R., Finnegan, R., Häusler, M., and Dzubay, A.: Structural Characterization of a Toppling Rock Slab From Array-Based Ambient Vibration Measurements and Numerical Modal Analysis, Journal of
450   Geophysical Research: Earth Surface, 127, https://doi.org/10.1029/2022JF006679, 2022.

Blair Jr, R. W.: Development of natural sandstone arches in south-eastern Utah., International geomorphology 1986. Proc. 1st conference. Vol. 2, 597–604, 1987.

Bottelin, P. and Baillet, L.: Original Insights Into Rock Slope Damage Processes Until Collapse From Passive Seismic Monitoring, Geophysical Research Letters, 51, e2024GL109139, https://doi.org/10.1029/2024GL109139, 2024.

455   Bottelin, P., Lévy, C., Baillet, L., Jongmans, D., and Guéguen, P.: Modal and thermal analysis of les arches unstable rock column (vercors massif, french alps), Geophysical Journal International, 194, 849–858, https://doi.org/10.1093/gji/ggt046, 2013a.

Bottelin, P., Jongmans, D., Baillet, L., Lebourg, T., Hantz, D., Levy, C., Le Roux, O., Cadet, H., Lorier, L., Rouiller, J.-D., Turpin, J., and Darras, L.: Spectral Analysis of Prone-to-fall Rock Compartments using Ambient Vibrations, Journal of
460   Environmental & Engineering Geophysics, 18, 205–217, https://doi.org/10.2113/JEEG18.4.205, 2013b.

Bottelin, P., Baillet, L., Larose, E., Jongmans, D., Hantz, D., Brenguier, O., Cadet, H., and Helmstetter, A.: Monitoring rock reinforcement works with ambient vibrations: La Bourne case study (Vercors, France), Engineering Geology, 226, 136–145, https://doi.org/10.1016/j.enggeo.2017.06.002, 2017.

Brincker, R. and Ventura, C.: Introduction to operational modal analysis, John Wiley and Sons, Inc, Chichester, West Sussex,
465   1 pp., https://doi.org/10.1002/9781118535141, 2015.

Brincker, R., Zhang, L., and Andersen, P.: Modal identification of output-only systems using frequency domain decomposition, Smart Mater. Struct., 10, 441–445, https://doi.org/10.1088/0964-1726/10/3/303, 2001.

Bruthans, J., Soukup, J., Vaculikova, J., Filippi, M., Schweigstillova, J., Mayo, A. L., Masin, D., Kletetschka, G., and Rihosek, J.: Sandstone landforms shaped by negative feedback between stress and erosion, Nature Geoscience, 7, 597–601, https://doi.org/10.1038/ngeo2209, 2014.

470

Burjánek, J., Gischig, V., Moore, J. R., and Fäh, D.: Ambient vibration characterization and monitoring of a rock slope close to collapse, Geophysical Journal International, 212, 297–310, https://doi.org/10.1093/gji/ggx424, 2018.

Burjánek, J., Kleinbrod, U., and Fäh, D.: Modeling the Seismic Response of Unstable Rock Mass With Deep Compliant Fractures, Journal of Geophysical Research: Solid Earth, 124, 13039–13059, https://doi.org/10.1029/2019JB018607, 2019.

475   Çelebi, M.: S2HM of Buildings in USA, Seismic Structural Health Monitoring: From Theory to Successful Applications, 3–30, https://doi.org/10.1007/978-3-030-13976-6_1, 2019.

Ceravolo, R., Pistone, G., Fragonara, L. Z., Massetto, S., and Abbiati, G.: Vibration-Based Monitoring and Diagnosis of Cultural Heritage: A Methodological Discussion in Three Examples, International Journal of Architectural Heritage, 10, 375–395, https://doi.org/10.1080/15583058.2013.850554, 2016.

480   Chopra, A. K.: Dynamics of structures: international edition, Pearson Education Limited, 2013.

Cimellaro, G. P. (Ed.): Seismic isolation, energy dissipation and active vibration control of structures. Volume 2, Corrected publication., Springer, Cham, 492 pp., 2023.

Clinton, J. F., Bradford, S. C., Heaton, T. H., and Favela, J.: The observed wander of the natural frequencies in a structure, Bulletin of the Seismological Society of America, 96, 237–257, https://doi.org/10.1785/0120050052, 2006.

485   Colombero, C., Baillet, L., Comina, C., Jongmans, D., and Vinciguerra, S.: Characterization of the 3-D fracture setting of an unstable rock mass: From surface and seismic investigations to numerical modeling, Journal of Geophysical Research: Solid Earth, 122, 6346–6366, https://doi.org/10.1002/2017JB014111, 2017.

Colombero, C., Baillet, L., Comina, C., Jongmans, D., Larose, E., Valentin, J., and Vinciguerra, S.: Integration of ambient seismic noise monitoring, displacement and meteorological measurements to infer the temperature-controlled long-term
490   evolution   of   a   complex   prone-to-fall   cliff,   Geophysical   Journal   International,   213,   1876–1897, https://doi.org/10.1093/gji/ggy090, 2018.

Colombero, C., Godio, A., and Jongmans, D.: Ambient Seismic Noise and Microseismicity Monitoring of a Prone-To-Fall Quartzite Tower (Ormea, NW Italy), Remote Sensing, 13, https://doi.org/10.3390/rs13091664, 2021a.

Colombero, C., Jongmans, D., Fiolleau, S., Valentin, J., Baillet, L., and Bièvre, G.: Seismic Noise Parameters as Indicators of
495   Reversible Modifications in Slope Stability: A Review, Springer Netherlands, 339–375 pp., 2021b.

Conati Barbaro, C., Fiorucci, M., Grechi, G., Forti, L., Marmoni, G. M., and Martino, S.: Safeguarding archaeological excavations and preserving cultural heritage in cave environments through engineering geological and geophysical approaches, Journal of Archaeological Science: Reports, 60, 104868, https://doi.org/10.1016/j.jasrep.2024.104868, 2024.

Cruikshank, K. M. and Aydin, A.: Role of fracture localization in arch formation, Arches National Park, Utah, Geological
500   Society of America Bulletin, 106, 879–891, https://doi.org/10.1130/0016-7606(1994)106<0879:ROFLIA>2.3.CO;2, 1994.

Doebling, S. W., Farrar, C. R., Prime, M. B., and Shevitz, D. W.: Damage identification and health monitoring of structural and mechanical systems from changes in their vibration characteristics: A literature review, 1996.

Dzubay, A., Moore, J. R., Finnegan, R., Jensen, E. K., Geimer, P. R., and Koper, K. D.: Rotational Components of Normal Modes Measured at a Natural Sandstone Tower (Kane Springs Canyon, Utah, U.S.A.), The Seismic Record, 2, 260–268, https://doi.org/10.1785/0320220035, 2022.

505

Farrar, C. R. and James III, G. H.: System identification from ambient vibration measurements on a bridge, Journal of Sound and Vibration, 205, 1–18, https://doi.org/10.1006/jsvi.1997.0977, 1997.

Finnegan, R., Moore, J. R., and Geimer, P. R.: Vibration of natural rock arches and towers excited by helicopter-sourced infrasound, Earth Surface Dynamics, 9, 1459–1479, https://doi.org/10.5194/esurf-9-1459-2021, 2021.

510   Finnegan, R., Moore, J. R., Geimer, P. R., Dzubay, A., Bessette-Kirton, E. K., Bodtker, J., and Vollinger, K.: Ambient Vibration Modal Analysis of Natural Rock Towers and Fins, Seismological Research Letters, 93, 1777–1786, https://doi.org/10.1785/0220210325, 2022.

Geimer, P. R., Finnegan, R., and Moore, J. R.: Sparse Ambient Resonance Measurements Reveal Dynamic Properties of Freestanding Rock Arches, Geophysical Research Letters, 47, https://doi.org/10.1029/2020GL087239, 2020.

515   Geimer, P. R., Finnegan, R., and Moore, J. R.: Meteorological Controls on Reversible Resonance Changes in Natural Rock Arches, Journal of Geophysical Research: Earth Surface, 127, https://doi.org/10.1029/2022jf006734, 2022.

Goodman, R. E.: Introduction to rock mechanics, Wiley, New York, 478 pp., 1980.

Habaraduwa Peellage, W., Fatahi, B., and Rasekh, H.: Stiffness and damping characteristics of jointed rocks under cyclic triaxial loading subjected to prolonged cyclic loading, International Journal of Fatigue, 181, 108121, 520   https://doi.org/10.1016/j.ijfatigue.2023.108121, 2024.

Häusler, M., Geimer, P. R., Finnegan, R., Fäh, D., and Moore, J. R.: An update on techniques to assess normal-mode behavior of rock arches by ambient vibrations, Earth Surface Dynamics, 9, 1441–1457, https://doi.org/10.5194/esurf-9-1441-2021, 2021a.

Häusler, M., Michel, C., Burjánek, J., and Fäh, D.: Monitoring the Preonzo Rock Slope Instability Using Resonance Mode 525   Analysis, Journal of Geophysical Research: Earth Surface, 126, https://doi.org/10.1029/2020JF005709, 2021b.

Iannucci, R., Martino, S., Paciello, A., D'Amico, S., and Galea, P.: Investigation of cliff instability at Għajn Ħadid Tower (Selmun Promontory, Malta) by integrated passive seismic techniques, Journal of Seismology, 24, 897–916, https://doi.org/10.1007/s10950-019-09898-z, 2020.

Ibrahim, S. R.: Random Decrement Technique for Modal Identification of Structures, Journal of Spacecraft and Rockets, 14, 530   696–700, https://doi.org/10.2514/3.57251, 1977.

Kleinbrod, U., Burjánek, J., and Fäh, D.: Ambient vibration classification of unstable rock slopes: A systematic approach, Engineering Geology, 249, 198–217, https://doi.org/10.1016/j.enggeo.2018.12.012, 2019.

Koper, K. D. and Hawley, V. L.: Frequency dependent polarization analysis of ambient seismic noise recorded at a broadband seismometer in the central United States, Earthquake Science, 23, 439–447, https://doi.org/10.1007/s11589-010-0743-5, 2010.

535   Kulatilake, P. H. S. W., Shreedharan, S., Sherizadeh, T., Shu, B., Xing, Y., and He, P.: Laboratory Estimation of Rock Joint Stiffness and Frictional Parameters, Geotechnical and Geological Engineering, 34, 1723–1735, https://doi.org/10.1007/s10706-016-9984-y, 2016.

Lazan, B. J.: Damping of materials and members in structural mechanics, 1968.

Lévy, C., Baillet, L., Jongmans, D., Mourot, P., and Hantz, D.: Dynamic response of the Chamousset rock column (Western
540 Alps, France), Journal of Geophysical Research: Earth Surface, 115, https://doi.org/10.1029/2009JF001606, 2010.

Lin, F. C., Li, D., Clayton, R. W., and Hollis, D.: High-resolution 3D shallow crustal structure in Long Beach, California:
Application of ambient noise tomography on a dense seismic array, Geophysics, 78, https://doi.org/10.1190/geo2012-0453.1,
2013.

Mayes, R. L., Rixen, D., Allen, M., and Rixen, D. J.: Conference Proceedings of the Society for Experimental Mechanics
545 Series, 2015.

McNamara, D. E. and Buland, R. P.: Ambiente noise levels in the continental United States, Bulletin of the Seismological
Society of America, 94, 1517–1527, https://doi.org/10.1785/012003001, 2004.

Mercerat, E. D., Payeur, J. B., Bertrand, E., Malascrabes, M., Pernoud, M., and Chamberland, Y.: Deciphering the dynamics
of a heterogeneous sea cliff using ambient vibrations: Case study of the Sutta-Rocca overhang (southern Corsica, France),
550 Geophysical Journal International, 224, 813–824, https://doi.org/10.1093/gji/ggaa465, 2021.

Moore, J. R., Geimer, P. R., Finnegan, R., and Thorne, M. S.: Use of Seismic Resonance Measurements to Determine the
Elastic Modulus of Freestanding Rock Masses, Rock Mechanics and Rock Engineering, 51, 3937–3944,
https://doi.org/10.1007/s00603-018-1554-6, 2018.

Moore, J. R., Geimer, P. R., Finnegan, R., and Michel, C.: Dynamic Analysis of a Large Freestanding Rock Tower (Castleton
555 Tower, Utah), Bulletin of the Seismological Society of America, 109, 2125–2131, https://doi.org/10.1785/0120190118, 2019.

Moore, J. R., Geimer, P. R., Finnegan, R., and Bodtker, J.: Between a beam and catenary: Influence of geometry on
gravitational stresses and stability of natural rock arches, Geomorphology, 364,
https://doi.org/10.1016/j.geomorph.2020.107244, 2020.

Müller, J. and Burjánek, J.: In situ estimation of effective rock elastic moduli by seismic ambient vibrations, International
560 Journal of Rock Mechanics and Mining Sciences, 170, 105459, https://doi.org/10.1016/j.ijrmms.2023.105459, 2023.

Ostanin, I., Safonov, A., and Oseledets, I.: Natural Erosion of Sandstone as Shape Optimisation, Sci Rep, 7, 17301,
https://doi.org/10.1038/s41598-017-17777-1, 2017.

Pau, A. and Vestroni, F.: Vibration assessment and structural monitoring of the Basilica of Maxentius in Rome, Mechanical
Systems and Signal Processing, 41, 454–466, https://doi.org/10.1016/j.ymssp.2013.05.009, 2013.

565 Řihošek, J., Slavík, M., Bruthans, J., and Filippi, M.: Evolution of natural rock arches: A realistic small-scale experiment,
Geology, 47, 71–74, https://doi.org/10.1130/G45421.1, 2018.

Riquelme, A. J., Abellán, A., Tomás, R., and Jaboyedoff, M.: A new approach for semi-automatic rock mass joints recognition
from 3D point clouds, Computers & Geosciences, 68, 38–52, https://doi.org/10.1016/j.cageo.2014.03.014, 2014.

Starr, A. M., Moore, J. R., and Thorne, M. S.: Ambient resonance of Mesa Arch, Canyonlands National Park, Utah,
570 Geophysical Research Letters, 42, 6696–6702, https://doi.org/10.1002/2015GL064917, 2015.

Taruselli, M., Arosio, D., Longoni, L., Papini, M., and Zanzi, L.: Seismic noise monitoring of a small rock block collapse test,
Geophysical Journal International, 224, 207–215, https://doi.org/10.1093/gji/ggaa447, 2021.

Van Overschee, P. and De Moor, B.: Subspace Identification for Linear Systems, Springer US, Boston, MA, https://doi.org/10.1007/978-1-4613-0465-4, 1996.

575 Welch, P.: The use of fast Fourier transform for the estimation of power spectra: A method based on time averaging over short, modified periodograms, IEEE Transactions on Audio and Electroacoustics, 15, 70–73, https://doi.org/10.1109/TAU.1967.1161901, 1967.

Zhang, W., Wang, J., Xu, P., Lou, J., Shan, B., Wang, F., Cao, C., Chen, X., and Que, J.: Stability evaluation and potential failure process of rock slopes characterized by non-persistent fractures, Nat. Hazards Earth Syst. Sci., 20, 2921–2935,
580 https://doi.org/10.5194/nhess-20-2921-2020, 2020.